Optical characterization of antimony-based bismuth-doped thin films with different annealing temperatures

Xinmiao Lu (逯鑫森)[1], Yiqun Wu (吴谊群)[1,2*], Yang Wang (王 阳)[1], and Jinsong Wei (魏劲松)[1]

[1]*Shanghai Institute of Optics and Fine Mechanics, Chinese Academy of Sciences, Shanghai 201800, China*

[2]*Key Lab of Functional Inorganic Material Chemistry, Ministry of Education, Heilongjiang University, Harbin 150080, China*

[*]*Corresponding author: yqwu@siom.ac.cn*

Received February 22, 2011; accepted April 28, 2011; posted online August 3, 2011

Antimony-based bismuth-doped thin film, a new kind of super-resolution mask layer, is prepared by magnetron sputtering. The structures and optical constants of the thin films before and after annealing are examined in detail. The as-deposited film is mainly in an amorphous state. After annealing at 170–370 °C, it is converted to the rhombohedral-type of structure. The extent of crystallization increased with the annealing temperature. When the thin film is annealed, its refractive index decreased in the most visible region, whereas the extinction coefficient and reflectivity are markedly increased. The results indicate that the optical parameters of the film strongly depend on its microstructure and the bonding of the atoms.

OCIS codes: 210.0210, 310.0310, 210.4245, 310.6860.

doi: 10.3788/COL201109.102101.

As demand for ultrahigh-density information storage continues to grow, the recording mark size in optical memory is reduced to the nanometer scale[1−4]. Exceeding the optical diffraction limit with traditional optical storage technology has become a challenge[5−6]. The super-resolution near-field structure technique which overcomes the limitations of optical diffraction and uses existing optical pickup systems was presented by Tominaga *et al*. in 1998. Consequently, the technique received considerable attention[5,7]. In this technique, functional film structures with proper mask layers are used to control the intensity profile of an incident laser spot to produce an aperture effect. Numerous mask layer materials have been studied[8−10]. Among them, antimony thin film with fast switching times is a promising candidate for mask layers. However, its threshold laser power of super-resolution readout is generally ∼4 mW[5], which is considerably higher than that of conventional discs (∼0.5 mW)[11]. Bismuth thin film with high nonlinear optical properties can concentrate energy into the center of a laser beam at low energy[12,13]. However, it is too sensitive to control. Antimony-bismuth thin film, a new kind of mask layer with excellent beam shaping, low threshold laser power, and high sensitivity for super-resolution readout, has been proposed in a Ref. [11]. The transport properties of antimony-bismuth in thin films and in bulk have been extensively studied because of their high thermoelectric efficiency at low temperatures[14,15]. To understand the super-resolution mechanism of the antimony-bismuth mask layer and extend its application as a new kind of optical thin film, its basic optical properties as well as the relationship between optical properties and structures must be studied.

In this letler, antimony-based bismuth-doped thin films are prepared by sputtering. The structures of the thin films deposited and annealed at different temperatures are investigated. Optical constants, including refractive index n and extinction coefficient k of the thin films, are reported. The relevance of the optical properties and structures of the film at different annealing temperatures are discussed.

The antimony-based bismuth-doped thin films were deposited on monocrystalline silicon substrates by direct current magnetron sputtering at room temperature using $Sb_{98}Bi_2$ (molar ratio) target with a purity of 99.99%. The background pressure was approximately 2.5×10^{-4} Pa, sputtering pressure was about 0.75 Pa of Ar environment, gas flow rate was 70 sccm, bias voltage was 0, and sputtering power was 30 W. Sputtering time was 181 s and the thickness of the thin film was approximately 100 nm. The thin film consisted of $Sb_{98.4}Bi_{1.6}$, which was determined by SEM/EDS (JSM-6360LA). The surface roughness of the thin film was characterized using an atomic force microscope (AFM, Multimode V, Veeco) in tapping mode. Figure 1 shows the AFM image of the as-deposited $Sb_{98.4}Bi_{1.6}$ film. Uniform and smooth film surface was obtained, the roughnesses of the film were $R_q = 1.41$ nm and $R_a = 1.10$ nm in the 5×5 μm area. Image processing and analysis were performed with the nanoscope software.

The thin films were annealed at 170, 270, and 370 °C

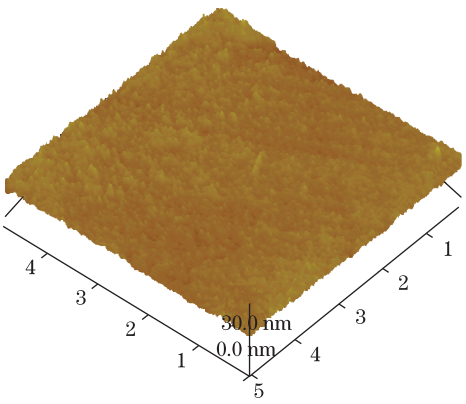

Fig. 1. AFM image of the as-deposited $Sb_{98.4}Bi_{1.6}$ film.

 © 2011 Chinese Optics Letters

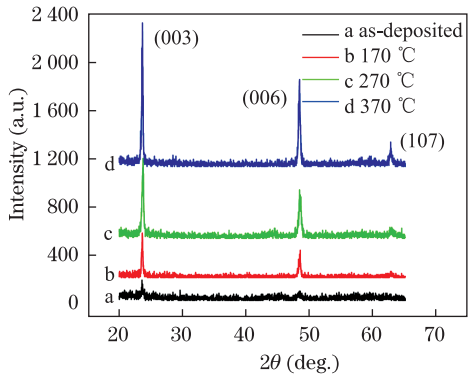

Fig. 2. XRD patterns of the as-deposited and annealed $Sb_{98.4}Bi_{1.6}$ thin films.

for 15 min. Heating rate was approximately 10 °C/min under a background pressure of 7.5×10^{-3} Pa. The structure of the thin films was studied by X-ray diffraction (XRD) (Ultima IV, Rigaku), scanning from 20° to 65°. The XRD patterns of the as-deposited and annealed films are shown in Fig. 2. Two very week peaks appeared at 23.54° and 48.27°. Few atoms were ordered in the as-deposited film. The structure of the as-deposited film was mainly in an amorphous state and a brief crystalline phase was observed. Compared with the as-deposited film, the intensity of the two peaks after annealing at 170° was considerably stronger. This shows that more atoms were ordered in the film after annealing, that is, the amorphous phase of the film was mostly converted to crystalline. The intensity of the peaks increased with the annealing temperature, especially at the peak of the (107) plane. This is evident in the pattern of the film annealed at 370 °C, but not in the pattern of the as-deposited film. The extent of crystallization increased with the annealing temperature. At the annealing temperature of 370 °C, almost all of the atoms in the film were aligned in a rhombohedral structure with the space group R-3m (166) and $Z = 4$.

Measurements of the optical constants (n and k) of the thin films were performed on an ellipsometer (GES5E, Sopra) at room temperature and 300–800 nm, with 5-nm interval. Sopra Winelli II modeling software was used to fit the data from the measurements. Incident linearly polarized light changes into elliptically polarized light after reflection. The polarization grade of reflected light is related to the refractive index $n(\omega)$ and extinction coefficient $k(\omega)$ of the material. The light incident on a surface of the thin film may be described by[16,17]

$$\overrightarrow{r_{\rm p}} = \frac{\overrightarrow{E_{\rm rp}}}{\overrightarrow{E_{\rm ip}}} = \frac{|E_{\rm rp}|}{|E_{\rm ip}|}\exp\left[{\rm i}\left(\theta_{\rm rp}-\theta_{\rm ip}\right)\right],$$
$$\overrightarrow{r_{\rm s}} = \frac{\overrightarrow{E_{\rm rs}}}{\overrightarrow{E_{\rm is}}} = \frac{|E_{\rm rs}|}{|E_{\rm is}|}\exp\left[{\rm i}\left(\theta_{\rm rs}-\theta_{\rm is}\right)\right], \quad (1)$$

where $\overrightarrow{r_{\rm p}}$ and $\overrightarrow{r_{\rm s}}$ are the p and s components of the complex reflective coefficients of the sample, respectively; $\overrightarrow{E_{\rm ip}}$ and $\overrightarrow{E_{\rm is}}$ are the p and s components of the incident wave, respectively, $\overrightarrow{E_{rp}}$, $\overrightarrow{E_{\rm rs}}$ are the p and s components of the reflected wave, respectively; and $|E_{\rm rp}|$, $|E_{\rm ip}|$, $|E_{\rm rs}|$, and $|E_{\rm is}|$ and $\theta_{\rm rp}$, $\theta_{\rm ip}$, $\theta_{\rm rs}$, and $\theta_{\rm is}$ are the absolute values and arguments of $\overrightarrow{E_{\rm rp}}$, $\overrightarrow{E_{\rm ip}}$, $\overrightarrow{E_{\rm rs}}$, and $\overrightarrow{E_{\rm is}}$, respectively. The components $\overrightarrow{E_{\rm rp}}$ and $\overrightarrow{E_{\rm rs}}$ constantly change in elliptically polarized light. To describe these characteristics, the ellipsometric parameters ψ and Δ are introduced as

$$\frac{\overrightarrow{r_{\rm p}}}{\overrightarrow{r_{\rm s}}} = \frac{|E_{\rm rp}/E_{\rm rs}|}{|E_{\rm ip}/E_{\rm is}|}\exp\left\{{\rm i}\left[\left(\theta_{\rm rp}-\theta_{\rm rs}\right)-\left(\theta_{\rm ip}-\theta_{\rm is}\right)\right]\right\}$$
$$= \tan\psi\exp\left({\rm i}\Delta\right), \quad (2)$$

$$\tan\psi = \frac{|E_{\rm rp}/E_{\rm rs}|}{|E_{\rm ip}/E_{\rm is}|}, \quad \Delta = \left(\theta_{\rm rp}-\theta_{\rm rs}\right)-\left(\theta_{\rm ip}-\theta_{\rm is}\right), \quad (3)$$

where $\tan\psi$ represents the relative change of the amplitude ratio of the p and s components of the complex reflective coefficients, and ψ and Δ are the elliptical azimuth and phase angle, respectively. As Eq. (3) shown, if $|E_{\rm ip}|/|E_{\rm is}| = 1$, ψ is determined only by the amplitude ratio of the p and s components of the reflected wave. If $\theta_{\rm rp}-\theta_{\rm rs} = 0$, Δ is determined only by the phase difference of the p and s components of the incident wave. The two points mentioned above can be verified in the experiment. The expressions of ellipsometric parameters ψ and Δ are

$$\tan\psi = |E_{\rm rp}|/|E_{\rm rs}|, \quad \Delta = -\left(\theta_{\rm ip}-\theta_{\rm is}\right). \quad (4)$$

The value of $\overrightarrow{r_{\rm p}}/\overrightarrow{r_{\rm s}}$ was determined from $\tan\psi$ and $\cos\Delta$. The plot of the parameters $\tan\psi$ and $\cos\Delta$ versus the wavelength for the as-deposited $Sb_{98.4}Bi_{1.6}$ thin film is shown in Fig. 3. The best-fit curves coincide well with the experimental data.

From the measured ellipsometric parameters $\tan\psi$ and $\cos\Delta$, the complex refractive index N ($N = n + {\rm i}k$) can be obtained by computational methods. In general, the real part n is related to the dispersion and the imaginary part k provides a measurement of dissipation rate of the electromagnetic wave in the film[18]. The reflectivity R of the films can be obtained from n and k[19]. The plots of n, k, and R against the wavelength are shown in Figs. 4–6.

The refractive index of the as-deposited film increased with wavelength linearly at 300–800 nm (Fig. 4). Index value was less than 1.48 in the ultraviolet region (300–400 nm), 1.48–2.28 in the blue-green region (400–590 nm), and 2.28–3.10 in the red-infrared region (600–800 nm). The slope of the n curve at 400–800 nm slightly increased after the film was annealed. The refractive index n curves of the

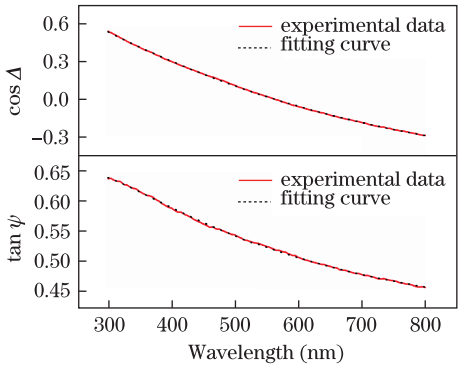

Fig. 3. Ellipsometric parameters $\tan\psi$ and $\cos\Delta$ versus the wavelength of the as-deposited $Sb_{98.4}Bi_{1.6}$ thin film.

as-deposited film crossed at 618, 634, and 754 nm when the thin films were annealed at 170, 270, and 370 °C, respectively. The curves red-shifted with higher annealing temperatures. Compared with the un-annealed $Sb_{98.4}Bi_{1.6}$ film, the value of n decreased at the wavelength region before the intersection points, but increased thereafter. The change of n increased with the annealing temperature, as the extent of crystallization of the film increased. After annealing at 370 °C, the n of the film in the crystalline state decreased at 300–750 nm, in contrast to that of the un-annealed film, which was mainly in an amorphous state. The values of n were lower at shorter wavelengths and decreased by 67% and 14% at 400 and 600 nm, respectively, but increased by 4.2% at 800 nm.

The extinction coefficient of the as-deposited film increased from 1.66 to 3.29 at 300 to 800 nm (Fig. 5). The value of k considerably increased after the film was annealed. Changes in the k value increased with the annealing temperature. After annealing at 370 °C, the k values of the film in the crystalline state increased by 39%, 60%, and 62% at 400, 600, and 800 nm, respectively, compared with those of the unannealed film. Changes in the k value of the film increased at longer wavelengths after crystallization in the visible wavelength region.

The reflectivity values of the as-deposited $Sb_{98.4}Bi_{1.6}$ thin film were 0.38–0.49 at 300–450 nm, and 0.49–0.55 at 450–800 nm (Fig. 6). At 450, the values of R increased by 39%, 47%, and 53% while at 800 nm, the values increased by 24%, 25%, and 31%, after annealing at 170, 270, and 370 °C, respectively. Moreover, the value of R

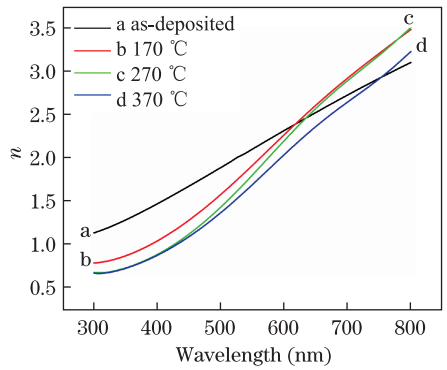

Fig. 4. Refractive index (n) curves of the $Sb_{98.4}Bi_{1.6}$ thin films.

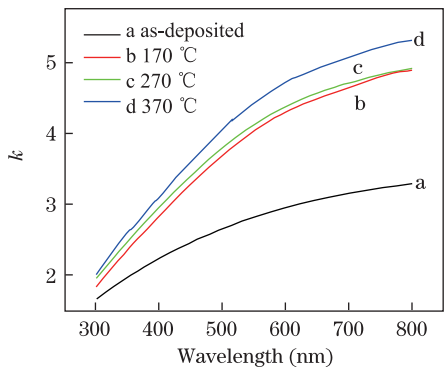

Fig. 5. Extinction coefficient (k) curves of the $Sb_{98.4}Bi_{1.6}$ thin films.

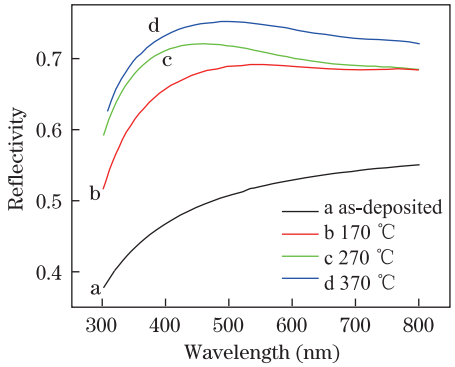

Fig. 6. Reflectivity R curves of the $Sb_{98.4}Bi_{1.6}$ thin films.

increased considerably after the film was annealed, and the changes in the value of R increased with the extent of crystallization. The variations of optical parameters of the films at different extents of crystallization after annealing are similar to those of other alloy thin films subjected to laser crystallization[20].

The constants of the films before and after annealing were very different, and showed strong dependence on the structures of the films. The refractive index is determined by the propagation velocity of light in the medium, which is affected by the interaction between light and the medium. For a light of single wavelength and vibration direction, the refractive index is determined by the microstructure of the material (or internal structure of the crystal). Thus, refractive index is an important parameter related to the microstructure of a material. The factors influencing the refractive index are as follows[20]. 1) The ionic radii of the elements in a material (refractive index increases with increasing ionic radius); 2) microstructure of a material, such as structures of the crystalline state and amorphous state; 3) internal stress in a material; 4) presence of allomorph. Generally, the refractive index of an allomorph is higher at lower temperatures.

For $Sb_{98.4}Bi_{1.6}$ thin films with a definite composition, the factors influencing the refractive index are mainly related to the microstructure of the film, including the structure of crystalline and amorphous states, transition of the film between the two states, and changes in the bonding of the atoms during structural change. The effect of the annealing temperature on crystallization was investigated by XRD (Fig. 2). A phase transition from the amorphous state to a rhombohedral-type structure occurred when the as-deposited $Sb_{98.4}Bi_{1.6}$ thin film was annealed. The as-deposited films generally contain a high concentration of unsaturated bonds or defects, which are responsible for the presence of the localized state in the amorphous band gap. During thermal annealing, the unsaturated bonds or defects are gradually reduced, thereby producing a large number of saturated bonds[21]. This decreases the density of localized states in the band. Subsequently, the atoms in the film rearrange from a disordered state in the amorphous film to an ordered state in the crystalline film with annealing. The extent of crystallization of the film increased with the annealing temperature, and the band gap of the film was reduced. This behavior is similar to those of most semiconductor alloy thin films[21,22]. The refrac-

tive index of the thin film decreases in the most visible wavelength region. The tendency of the refractive index of the thin film to vary with the annealing temperature is in agreement with the change in the extent of crystallization. The changes in the extinction coefficient and reflectivity of the film are due to its structural changes before and after annealing. The changes in the bonding of the atoms in the process of structure transition play an important role on the value of the extinction coefficient. The effects are opposite to those of the refractive index. In the present study, dissipation rate of the electromagnetic wave in the crystallization film was higher than that in the amorphous film. The extinction coefficient of the film greatly increased after annealing at 30–800 nm. The reflectivity was closely related to the microstructure of the film, and strongly influenced by phase transition. This was also enhanced with the increased extent of crystallization. These observations concur with the structural changes of the film during thermal annealing.

In conclusion, antimony-based bismuth-doped $Sb_{98.4}Bi_{1.6}$ thin films are deposited on single crystalline silicon substrates by direct-current magnetron sputtering method. The surface and crystal structures of the as-deposited and annealed films at different temperatures are investigated. The optical constants, n and k, of the thin films before and after annealing are studied. The results show that the structure of the as-deposited film is mainly in an amorphous state and a brief crystalline phase is achieved. The amorphous state of the film is mostly converted to the crystalline state after annealing at 170 °C, and the extent of crystallization increases with the annealing temperature. After annealing at 370 °C, the crystalline state with a rhombohedral type structure is formed. The optical parameters of the film strongly depend on the microstructure of the film (including the crystalline and amorphous structure), the transition of the film between the two states, and changes in the bonding of the atoms in the film.

This work was partially supported by the National Basic Research Program of China (No. 2007CB935402) and the National Natural Science Foundation of China (Nos. 50872139 and 60644002).

References

1. F. Gan, J. Non-Cryst. Solids **354,** 1089 (2008).
2. S. Raoux, W. Welnic, and D. Ielmini, Chem. Rev. **110,** 240 (2010).
3. K. Narumi, T. Akiyama, N. Miyagawa, T. Nishihara, H. Kitaura, R. Kojima, K. Nishiuchi, and N. Yamada, Jpn. J. Appl. Phys. Part 1 **41,** 2925 (2002).
4. H. Ding, L. Dai, and C. Yan, Chin. Opt. Lett. **8,** 706 (2010).
5. J. Tominaga, T. Nakano, and N. Atoda, Appl. Phys. Lett. **73,** 2078 (1998).
6. V. F. Canales, P. J. Valle, J. E. Oti, and M. P. Cagigal, Chin. Opt. Lett. **7,** 720 (2009).
7. H. S. Lee, T. S. Lee, Y. Lee, J. Kim, S. Lee, J. Y. Huh, D. Kim, and B. K. Cheong, Appl. Phys. Lett. **93,** 221108 (2008).
8. L. Shi, T. C. Chong, P. K. Tan, J. Li, X. Hu, X. Miao, and Q. Wang, Jpn. J. Appl. Phys. Part 1 **44,** 3615 (2005).
9. Q. Liu, J. Kim, T. Fukaya, and J. Tominaga, Opt. Express **11,** 2646 (2003).
10. W.-C. Liu, C.-Y. Wen, K.-H. Chen, W. C. Lin, and D. P. Tsai, Appl. Phys. Lett. **78,** 685 (2001).
11. L.-X. Jiang, Y.-Q. Wu, Y. Wang, J.-S. Wei, and F.-X. Gan, Chin. Phys. Lett. **26,** 024214 (2009).
12. F. Zhang, W. Xu, Y. Wang, and F. Gan, Solid State Commun. **134,** 375 (2005).
13. D. R. Liu, K. S. Wu, M. F. Shih, and M. Y. Chern, Opt. Lett. **27,** 1549 (2002).
14. X. Devaux, F. Brochin, R. Martin-Lopez, and H. Scherrer, J. Phys. Chem. Solids **63,** 119 (2002).
15. S. Cho, A. DiVenere, G. K. Wong, J. B. Ketterson, and J. R. Meyer, Phys. Rev. B **59,** 10691 (1999).
16. R. M. A. Azzam and N. M. Bashara, *Ellipsometry and Polarized Light* (North-Holland, 1977).
17. Q. Chen, D. Gu, and F. Gan, Physica B **212,** 189 (1995).
18. X. Y. Li, Y. Q. Wu, D. D. Gu, and F. X. Gan, Mater. Sci. Eng. B-Adv. Funct. Solid-State Mater. **158,** 53 (2009).
19. T. Yuan, Y. Huang, S. Dong, T. Wang, and M. Xie, Polym. Test. **21,** 641 (2002).
20. B. Liu, H. Ruan, and F. Gan, Chin. J. Semicond. (in Chinese) **23,** 479 (2002).
21. S. A. Khan, J. K. Lal, and A. A. Al-Ghamdi, Opt. Laser Technol. **42,** 839 (2010).
22. E. A. El-Sayad, B. S. Farag, and L. I. Soliman, J. Phys. D: Appl. Phys. **42,** 225401 (2009).